Electrophysiologically Informed Neuromorphic Spiking Networks for Spatial Navigation

Lear Cohen, Hadar Cohen Duwek, Elishai Ezra Tsur*

Neuro-biomorphic Engineering Lab (NBEL)
The Open University of Israel
* elishai@nbel-lab.com

Abstract

Spatial memory underlies the mental encoding, storage, and retrieval of spatial representations that support navigation in intricate environments. Conventional models of navigation accentuate the role of place and grid cells as principal neural substrates. However, recent findings in teleost fish, the most diverse vertebrate class, suggest that navigation in these species depends primarily on boundary vector cells (BVCs) and hydrostatic pressure (HP) cues. In this study, we designed a neuromorphic spiking neural network (SNN) for spatial navigation, directly informed by electrophysiological recordings from the goldfish telencephalon. Within this architecture, BVC populations mediated obstacle avoidance, while HP-sensitive units provided a vertical reference for goal-oriented trajectory planning. Our results demonstrate that efficient navigation can emerge without explicit positional coding, consistent with experimental observations of low firing rates and limited neuronal populations in the fish telencephalon. The proposed framework thus establishes a compact and biologically grounded model for fish-inspired neuromorphic navigation that remains robust and scalable across naturalistic conditions.

Introduction

The ability to navigate is fundamental and crucial for the survival of almost all animal species. It includes neuronal representation of self, others and salient features in the environment. The cell types comprising this neuronal system were investigated in many model animals (Cohen et al. 2023; Finkelstein et al. 2016; Moser et al. 2008; O'Keefe and Dostrovsky 1971; Payne et al. 2021). Among them, place cells (Geva-Sagiv et al. 2015) and grid cells (Rowland et al. 2016) were found to be common to multiple species, enabling them to derive current position and odometry. Therefore, they were used in multiple studies aiming to model the neural navigation system (Dumont and Eliasmith 2020; Komer and Eliasmith 2020; Zhao and Si 2025). However, studying navigation in natural environments revealed a distinctive picture: place cells had a non-typical spatial tuning in large environments (Eliav et al. 2021), and the 2D hexagonal symmetry of grid cells was not as expected in 3D environments (Ginosar et al. 2021). Hence, more complex models were suggested to enable natural navigation (Ginosar et al. 2023; Zhao and Si 2025).

Fish represent the most diverse and abundant vertebrate lineage. Both laboratory and field studies have demonstrated that they navigate successfully using allocentric and egocentric reference frames (Broglio et al. 2011; Rodriguez et al. 1994), as well as by retracing learned routes to feeding locations over multiple days (Givon et al. 2022). Electrophysiological recordings from the goldfish telencephalon revealed that, unlike mammals, fish lack conventional place and grid encoding schematics. Instead, their spatial representation appears to rely on boundary vector cells (BVCs; Cohen et al. 2023), which encode both distance and direction from salient environmental boundaries. Additional behavioral and physiological findings (Davis et al. 2021; Givon et al. 2025; Cohen 2023) indicate that fish also exploit hydrostatic pressure (HP) as a vertical positional cue, complementing other kinematic encoders such as speed, velocity, and head-direction cells (Vinepinsky et al. 2020). Despite their relatively low neuronal firing rates and smaller populations, these mechanisms may be sufficient to support robust spatial navigation.

The precise biological basis for distance estimation via BVCs and for depth sensing from HP cues remains unresolved. Several mechanisms for aquatic depth perception have been proposed, including visual parallax (Pedraja et al. 2018) and optical flow (Kubo et al. 2014), both of which enable estimation of distance from nearby surfaces. Fish also possess a lateral line system that detects hydrodynamic pressure gradients (Ristroph et al. 2015), allowing detection of nearby boundaries through flow perturbations. Moreover, the swim bladder - an air-filled organ that changes volume with HP variations - provides an additional sensory route linked to the inner ear (Taylor et al. 2010; Baxendale and Whitfield 2014; Schulz-Mirbach et al. 2013), implicating auditory pathways in positional coding. Fish can also rely

on spatial memory and path integration (McNaughton et al. 2006), as evidenced by their ability to learn spatial layouts and take shortcuts to targets (Sibeaux et al. 2024).

To explore these mechanisms, we developed a neuromorphic spiking neural network (SNN) modeled after the goldfish navigation system. Unlike conventional artificial neural networks, SNNs transmit information through discrete spiking events, offering higher biological plausibility (Tsur 2021). Our framework follows the Neural Engineering Framework (NEF; Eliasmith and Anderson 2003), implemented in Nengo (Bekolay et al. 2014), which provides a computational substrate for realistic sensory-motor and cognitive modeling (Cohen-Duwek and Ezra Tsur 2021; Cohen-Duwek, Slovin, and Ezra Tsur 2022). Previous NEF-based navigation systems (Conklin and Eliasmith 2005; Dumont, Orchard, and Eliasmith 2022) were largely inspired by mammalian hippocampal navigation; here, we extend this approach to an aquatic species.

We implemented four NEF-based navigation models capturing the goldfish's natural strategy. Neural parameters were derived from experimental recordings in the telencephalon, including realistic tuning curves and population sizes. The simulated circuit comprised BVC, HP, and kinematic units encoding speed and head direction. We tested several navigation strategies, random direction, following a known initial azimuth, and HP-driven vertical localization. To maintain biological realism, sensory modules were treated as black boxes: rather than simulating each sensory modality, the virtual agent's spatial position was used to define corresponding visual boundary inputs and HP cues outside the simulation loop. These cues enabled goal-directed navigation without explicit access to the agent's 3D coordinates or odometry.

Methods

Experimental Setup

The electrophysiological datasets (Cohen et al. 2023; Vinepinsky et al. 2020) underlying our models were derived from recordings in the goldfish telencephalon, a region considered homologous to the mammalian hippocampus. In these studies, a wireless recording implant encased in a waterproof housing was chronically positioned in the telencephalon, allowing extracellular recordings during free exploration. Fish swam for 90 min in shallow or vertical quasi-2D arenas without explicit goals or reinforcement. The shallow arenas were rectangular (60 × 60 × 20 cm) or circular (69 cm diameter, 20 cm depth), each included distinct visual wall cues. In some control sessions, the entire arena was rotated to examine spatial remapping. Recordings revealed multiple cell types: edge cells, activated near environmental boundaries, as well as head-direction, speed, and velocity cells tuned to motion parameters. Vertical environments (70 × 20 × 70 cm; Fig. 1A, right) incorporated a natural hydrostatic-pressure (HP) gradient absent in earlier study. Additional sessions examined the effects of geometry or pressure manipulations, such as adding a vertical shelf or altering water level while preserving the visual scene. These experi-

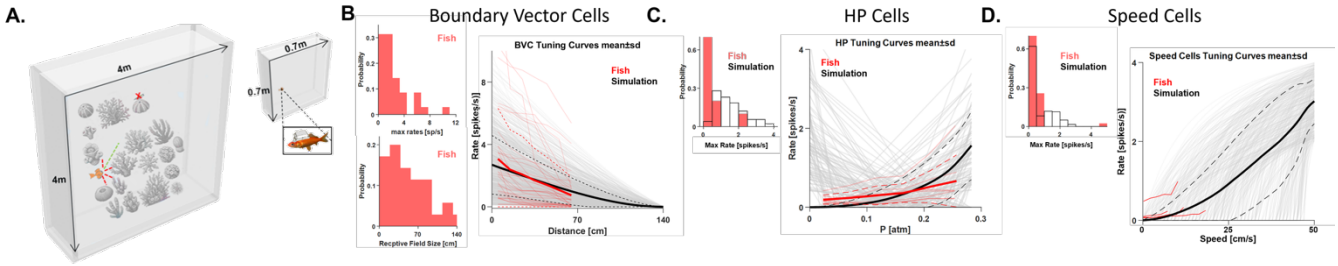

Figure 1 | Biologically inspired modeling of the goldfish navigation system. **A.** Left: schematic illustration of the simulated virtual arena. Dashed vectors represent examples of BVC activation—red vectors indicate the directions and distances to nearby obstacles, whereas the green vector marks a potential unobstructed trajectory. The red "×" denotes the target location. Right: configuration of the behavioral arena used in the reference goldfish electrophysiology experiments (Cohen et al. 2023).**B.** Comparison between empirically recorded and simulated BVC characteristics. Left: distributions of maximal firing rates (top) and receptive-field widths (bottom) derived from Cohen et al. (2023). Right: empirical BVC tuning curves (thin blue lines) plotted against the corresponding modeled curves (thin gray lines). Thick solid and dashed lines indicate population means and standard deviations, respectively. **C.** Hydrostatic-pressure (HP) cell properties from Cohen (2023) and their Nengo implementation. Left: maximal firing-rate distributions of recorded (blue) and modeled (black) neurons. Right: firing-rate tuning functions to HP stimuli, showing biological (blue) versus simulated (gray) curves.**D.** Speed-cell data from Vinepinsky et al. (2020) using the same plotting conventions as panel C.

ments revealed boundary-vector cells (BVCs) encoding distance and direction to salient features, and HP-sensitive neurons encoding depth information.

Virtual Navigation Task

We replicated the experimental conditions in a digital twin simulation (Fig. 1A), scaling the arena ×32 to a 4 × 4 m virtual environment. The agent's start position (home zone) and target (analogous to a food site) were placed in opposite quadrants. Between 20 and 30 circular obstacles (radius 0.15 m) were randomly distributed, forming a coral-like maze reminiscent of natural foraging habitats. The agent's objective was to reach the target rapidly while avoiding collisions, with a maximum velocity of 0.5 m/s.

Neuron Types and Characteristics

The simulated navigation circuit was constructed from biologically grounded components recorded in goldfish: BVC and HP units representing spatial cues, and speed, head-direction (HD), and velocity units representing kinematic cues. For BVC modeling, empirically recorded firing-rate tuning curves (Cohen et al. 2023) were used to parameterize distance-dependent activity. We fitted skew-normal distributions to describe peak firing rates and receptive-field widths and used these to synthesize artificial populations with matched intercepts and amplitudes (Fig. 1B).

The spiking implementation used Nengo's Rectified Linear neurons, whose linear tuning better reflected the monotonic BVC profiles observed in fish compared to standard leaky integrate-and-fire (LIF) neurons. Directional sensitivity was implemented through an ensemble array, each sub-ensemble representing a distinct direction (15° resolution, uniformly distributed). An analogous procedure was used for HP neurons (Fig. 1C), reproducing their depth-related tuning curves. Speed, HD, and velocity cells (Fig. 1D) were modeled with LIF neurons whose amplitude parameters matched the low firing rates (0.1–4 spikes/s) characteristic of the goldfish telencephalon. Population sizes were scaled according to the empirical proportions of each cell type (Cohen et al. 2023; Vinepinsky et al. 2020), assuming a total navigation network of ~10,000 neurons. Of 196 recorded units, 35 (≈ 17.9 %) were BVCs, yielding 1,785 modeled BVCs; the remaining cell classes (speed, HD, velocity) each comprised ~1,500 neurons.

Navigation Strategies

To address the virtual navigation task, several strategies were implemented. As a baseline (null) condition, the agent selected an initial heading at random within ±45° of the actual target direction. Its trajectory was modified only upon encountering an obstacle, with no explicit knowledge of the target's position. Speed regulation and collision avoidance were governed by the BVC ensembles as described above and remained consistent across all models. In the Azimuth model, the agent was provided with the initial target azimuth while maintaining all other conditions identical to the baseline. In contrast, the hydrostatic-pressure (HP) model incorporated an additional constraint: the agent was initialized with prior knowledge of the target's HP value, effectively representing its vertical coordinate. The agent first ascended or descended until reaching this HP level and subsequently updated its azimuthal heading to 0° or 180°, depending on the relative start–target alignment. This strategy follows behavioral findings in goldfish navigation (Givon et al. 2025). The HP-max model utilized Nengo's default leaky integrate-and-fire (LIF) neurons with higher maximal firing rates (400 spikes/s) and a tenfold increase in neuronal count to evaluate performance scalability.

NEF-Based Navigation

The Neural Engineering Framework (NEF) (Eliasmith and Anderson 2003) provides a systematic approach for building biologically plausible spiking neural networks that can represent, transform, and maintain information over time. It is grounded on three main principles: representation, transformation, and dynamics. Representation defines how information is encoded by populations of neurons. For a neural population, the activity of neuron i at time t is given by:

$$a_i(t) = G_i(\alpha_i \langle \vec{e}_i, \vec{x}(t) \rangle + J_i^b)$$

where G_i is the neuron model (for example, LIF), α_i is the gain factor, e_i is the preferred direction of neuron i, and J_i^b is the bias current. Transformation describes how functions of represented variables are computed through weighted connections between neurons. The decoded estimate of a function $\boldsymbol{f}(\vec{\boldsymbol{x}})$ is given by:

$$\hat{f}(\vec{x}) = \sum_i a_i(t) \cdot d_i$$

where d_i are decoding weights optimized to approximate the target function. Dynamics refers to how recurrent neural connections generate temporal evolution of represented states according to differential equations. For a general dynamic system:

$$\frac{d\vec{x}(t)}{dt} = f(\vec{x}(t)) + \vec{u}(t)$$

where $\vec{\boldsymbol{u}}(\boldsymbol{t})$ represents the external input signal. Recurrent feedback within the NEF is defined by:

$$f_r(x) = \tau \cdot f(x) + x$$

where τ is the synaptic time constant introducing low-pass filtering of the signal (Izhikevich 2007). This formulation

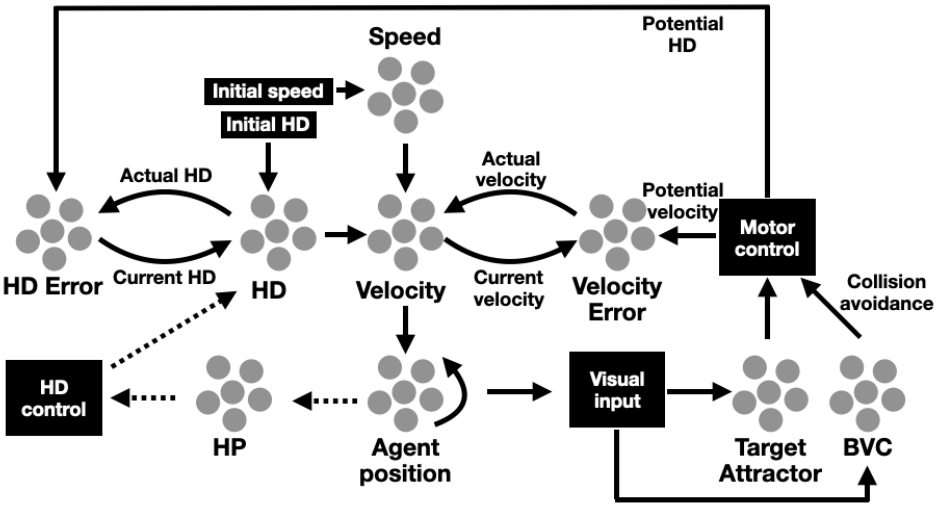

Figure 2. Neural Engineering Framework (NEF)-based model of the goldfish navigation system. A. Schematic diagram of the Nengo-based architecture replicating the fish's navigation circuitry. Cell classes correspond to those shown in Figure 1A. Dotted clusters represent neuron ensembles, while rectangular frames denote external input nodes supplying sensory information to the network. Dotted arrows indicate HP control model.

enables the network to approximate continuous dynamical systems through decoded neural activity and feedback.

Using this framework, we implemented two canonical dynamical systems: an integrator and an attractor. The integrator accumulates input over time via recurrent connections, enabling continuous estimation of motion or position variables. The attractor network defines stable states in neural space, toward which activity naturally converges, supporting short-term memory and decision processes. Both mechanisms exploit NEF's capability to map mathematical system equations onto recurrent spiking architectures.

Biologically Inspired Navigation Model

The navigation framework was implemented in the Nengo simulator, combining boundary vector cell (BVC) and hydrostatic pressure (HP) mechanisms to replicate goldfish-like spatial navigation (Fig. 2). BVC ensembles encoded the egocentric distance and direction to nearby obstacles, whereas HP-sensitive populations provided a vertical reference for estimating depth. The overall objective of the system was to guide the agent within a bounded 2D arena, enabling obstacle avoidance and efficient trajectory planning toward a goal. The model received as inputs the agent's initial speed and orientation, which were represented by speed and head-direction (HD) ensembles. These were combined in velocity neurons, encoding the instantaneous velocity vector according to:

$$\vec{v}(t) = s(t) \cdot \left[cos\left(\theta(t)\right), sin\left(\theta(t)\right)\right]$$

where s(t) is the instantaneous speed and θ(t) is the heading direction. The velocity output was then projected to a neural integrator that maintained a continuous estimate of the agent's position over time.

The visual scene, defined externally, was represented by an array of BVC ensembles and an additional attractor ensemble encoding target-related cues. The BVC activity guided the selection of clear paths, while the attractor network was activated only when the target was within the visual field. The combined motor-control signal was translated into updates of the agent's velocity and head-direction populations by minimizing the difference between desired and current neuronal activity patterns. In models employing HP-based strategies, the integrator's output was also fed into an HP ensemble encoding the agent's current pressure level. This signal modulated the head-direction system, aligning the agent's heading toward the target's vertical coordinate until the correct HP value was reached. A schematic overview of the full computational architecture is shown in Figure 2, with detailed model parameters provided in the subsequent section.

Computational Model

The virtual navigation task began with the agent positioned in a 4 × 4 m square arena. Its initial motion speed was $S_0(t) = v_{max} = 0.5$ m/s, encoded by the speed-cell ensemble, while the initial head direction (HD) was defined according to the chosen navigation strategy. The agent's translational velocity was expressed as:

$$\vec{v}(t) = \left(v_x(t), v_y(t)\right) = s(t) \cdot \left[cos\left(\theta(t)\right), sin\left(\theta(t)\right)\right]$$

where s(t) denotes instantaneous speed and θ(t) the heading direction. Velocity was encoded by a third population, the

velocity-cell ensemble. Neural connections in Nengo were implemented with biologically realistic synaptic time constants acting as low-pass filters. A constant of τ_1 = 20 ms was used for speed–HD integration into velocity encoding, and τ_2 = 100 ms for the position integrator implementing: $\boldsymbol{d\vec{p}(t)/dt = \vec{v}(t)}$. In NEF, this integration is achieved via a recurrent connection with identity feedback and scaled input (τ_2) to convert velocity units from [m/s] to [m]. Although this ensemble represented position, it was not modeled as hippocampal place cells; instead, LIF neurons (n = 1500) with low firing rates ($\leq$ 4 spikes/s) were used. The positional output defined the visual scene and HP-cell inputs, rather than serving for direct navigation.

In the HP and HP-max models, the vertical position component was sent to the HP ensemble (τ_1), which relayed a binary signal to the HD-control node indicating whether the target was shallower or deeper. Once the HP difference fell below 0.2 m, the HD-control switched orientation to 0° (right) or 90° (left) based on initial alignment.

All models were implemented in Nengo 4.0.0 using Python 3.9, and executed on an NVIDIA A100 GPU (80 GB RAM).

Visual input, target attractor, and boundary vector cell

The visual scene node was externally defined to approximate vision as a black-box input. While several studies model visual processing in teleosts (Ecke et al. 2020; Fernandes et al. 2021; Northmore 2024; Rosa Salva et al. 2014), here it was simplified to preprocessed inputs describing obstacle and target distances. At each time step, the scene provided: Distances to all obstacles (corals) within 1.4 m, and Distance to the target. These signals were propagated to both the BVC system and a target attractor, a binary variable denoting target visibility. When the target became visible, a motor command triggered a direct movement toward it.

The attractor dynamics followed:

$$\frac{d\vec{p}(t)}{dt} = \vec{v}(t) + \vec{G}(t)$$

where

$$\vec{G}(t) = \begin{cases} \vec{g} - \vec{p}(t), & if\ \|\vec{g} - \vec{p}(t)\| < r_{vis}; \\ 0, & otherwise \end{cases}$$

and r_{vis} = 0.3 m defines the visual radius. BVCs modeled egocentric boundaries with an angular resolution $\Delta\theta$ = 15°, producing N_BVC = 24 directional bins. Each coral (radius r_coral) subtended an angular aperture 2·arctan(r_coral / d), where d is the Euclidean distance from agent to coral center. For each affected bin, the corresponding distance $d_i(t)$ was computed, and the BVC sensory signal defined as:

$$BVC_i(t) = f(d_i(t)) \text{ , } i = 1 \ldots N\_BVC$$

Both BVC and attractor outputs were then fed into the motor-control system, producing a potential velocity vector that guided the agent until the target was reached. Simulations terminated upon success or after 45 s if the goal remained unreached.

Motor Control

Distance and direction encoding for obstacle avoidance followed previous LiDAR-based navigation models (Shalumov et al. 2021). The LiDAR input, comprising paired vectors of object distance and angle, served as input to a decision-making circuit involving Nengo's Basal Ganglia (BG) and Thalamus modules (Stewart et al. 2010).

This approach parallels subpallial structures in fish (Bloch et al. 2020; Mueller 2012; Wullimann 2011), which project to the pallium, a hippocampal analog essential for spatial control (Northcutt 2011; Rodriguez et al. 2002). The BG–Thalamus model enabled dynamic speed adjustment and smooth steering (Fig. 2B). Relative obstacle distance was computed as: $\hat{d} = (d - \varepsilon) / (D - \varepsilon)$,
where ε = 0.03 m (safety margin) and D = 0.4 m (critical slowdown threshold). The agent's speed along each spatial axis $a \in \{x, z\}$ was defined as:

$$v_a^{new} = \begin{cases} \min\left((|v_a| + v_\epsilon) \cdot \hat{d}, |v_a| \right) & if\ d < D; \\ min(v_a + d_c \cdot \tau_2, v_{max}) & otherwise \end{cases}$$

where $\boldsymbol{d_c}$ = 3 m/s² is the deceleration coefficient. The potential velocity component was then:

$$v_a^{potential} = sign(v_a) \cdot min\left(max(|v_a^{new}|, 0), v_{max}\right)$$

When frontal obstacles blocked the path ($d_0(t) < D$), BVC outputs were processed by the BG–Thalamus circuit to compute a steering angle θ_steer, determining the optimal turn within $\theta \in [-\pi/2, \pi/2]$: $\boldsymbol{\theta_{steer} = \alpha \cdot \theta_{new} + (1 - \alpha)\theta_{old}}$, with α = 0.9. The potential velocity vector was rotated accordingly:

$$\boldsymbol{\vec{v}_{potential} = R(\theta_{steer}(t)) \cdot v_{allocentric}(t)}$$

where R(θ) is the 2D rotation matrix: R(θ) = [[cosθ, −sinθ], [sinθ, cosθ]]. Velocity and head-direction signals were continuously corrected via low-pass filtered error terms:

$$\vec{v}_{error} = \vec{v}_{potential}(t) - \vec{v}_{current}(t)$$
$$HD_{error} = HD_{potential}(t) - HD_{current}(t)$$

The actual outputs evolved according to:

$$\frac{d\vec{v}_{actual}(t)}{dt} = \frac{1}{\tau_2}(\vec{v}_{error} - \vec{v}_{actual}(t))$$

$$\frac{dHD_{actual}(t)}{dt} = \frac{1}{\tau_2}(HD_{error}(t) - HD_{actual}(t))$$

This configuration ensured smooth, biologically plausible trajectory updates throughout navigation.

Power Analysis

Each navigation strategy was tested across five environments, repeated ten times each (Fig. 3A-E). For each strategy, trajectories were resampled to uniform length, and inter-trajectory distances were computed using MATLAB's Dynamic Time Warping (DTW). Smaller distances indicated higher consistency across repetitions. Distributions were compared via t-tests. (1) Target Reached and Success Rate: A successful trial (value = 1) was defined as one where the target was reached. The success rate was the fraction of successful trials per condition. Error bars were obtained via 100 bootstrap iterations estimating mean ± standard error. (2) Time to Target: A normalized estimate in [0, 1], where 0 represents the minimal possible travel time (straight-line distance / maximal speed) and 1 corresponds to 45 s (simulation limit). Trials that failed to reach the target were excluded. (3) Distance Traveled: Total travel distance was normalized such that 0 represents the shortest Euclidean path and 1 equals the maximum possible travel (45 s × 0.5 m/s). Unsuccessful trials were excluded. (4) Collision Rate: The collision rate was computed as the proportion of time steps where the agent's distance to any coral center was less than its radius (0.15 m), yielding a value between 0 and 1. (5) Total Score: A combined metric in [0, 1] summarizing overall navigation performance:

TotalScore = TargetReached × ((1 − TimeToTarget) + (1 − DistanceTraveled) + (1 − Collisions)) / 3.

Results

To evaluate the performance of the different navigation strategies, we simulated six environments, each tested ten times under four models: (1) Null model, serving as a reference with no directed strategy; (2) Azimuth model, where the agent was initialized with the target's azimuth; (3) HP model, where the agent also knew the hydrostatic pressure (HP) corresponding to the target's depth; and (4) HP_{max} model, identical to the HP model but featuring a 100-fold increase in firing rates and a tenfold larger neural population. An example of one virtual environment is shown in Figure 3A–D.

After each simulation set, we quantified the trajectory similarity within each strategy by computing the summed

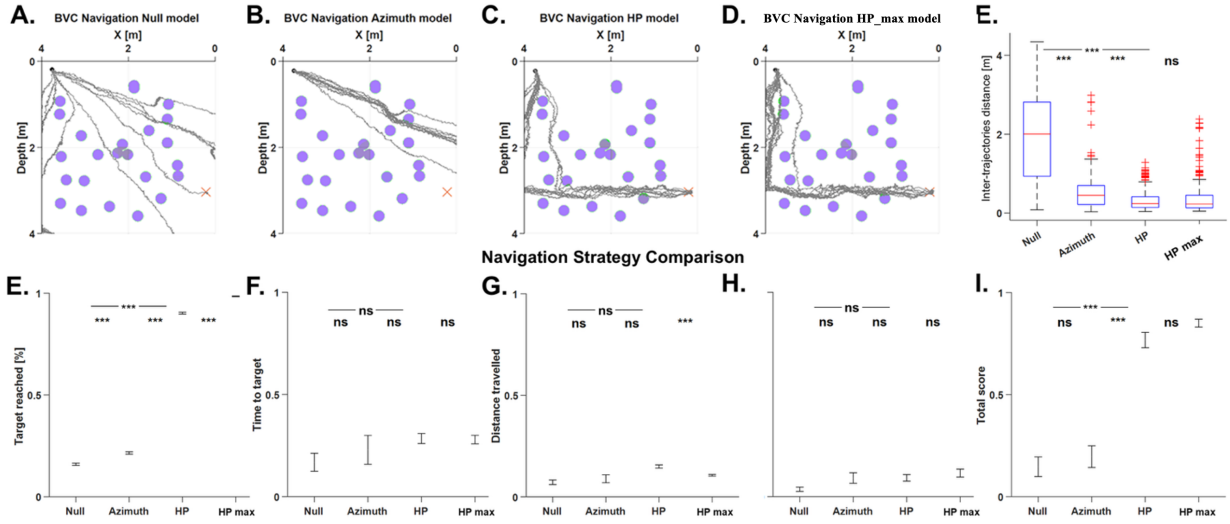

Figure 3 | Power analysis and model comparison. A–D. Example trajectories (gray lines) generated by the agent across identical environments when using different navigation strategies: **A.** Null model, **B.** Azimuth model, **C.** HP model, and **D.** HP_{max} model. In each panel, the red "×" marks the target position. **E.** Mean ± SD of inter-trajectory distances across all strategies, aggregated over six environments. Smaller distances indicate higher reproducibility. ***$p < 10^{-4}$ (t-test) shows that the HP model yielded significantly greater trajectory consistency than the Null and Azimuth models. **F–I.** Performance comparison metrics for the four navigation strategies (Null, Azimuth, HP, HP_{max}): **F.** Proportion of successful trials (n = 50 simulations), **G.** Normalized time to reach the target, **H.** Normalized travel distance, and **I.** Collision rate during navigation. Error bars represent mean ± SE. ns = $p > 0.05$; * $p < 10^{-2}$; ** $p < 10^{-3}$; *** $p < 10^{-4}$. The HP model significantly outperformed the Null and Azimuth models and not outperformed the HP_{max} model.

stepwise Euclidean distances (see Methods) across all possible trajectory pairs (n = 45) from ten repetitions. These values, aggregated across all six environments, are presented in Figure 3E, where smaller values indicate higher similarity among trials. The HP model showed significantly greater consistency than both the Null and Azimuth models ($p < 10^{-4}$, t-test), demonstrating that integrating HP cues stabilizes navigation. Notably, the HP_{max} model, despite its much higher firing rates and larger neuronal population, did not outperform the HP model, underscoring the computational efficiency of the simpler, biologically constrained configuration. To further assess strategy performance, we tested each model across 50 randomized environments differing in start position, goal location, and obstacle layout. Four normalized behavioral metrics were computed (see Methods): Target reached, time to target, distance traveled, and collision rate, which together formed a composite performance score. These results are summarized in Figure 3F–I. Although the Null and Azimuth models occasionally reached the goal, their performance remained inconsistent. In successful trials, travel time and path length did not differ significantly from the HP model, yet the overall performance score was substantially higher for the HP strategy ($p < 10^{-4}$, t-test). Collision rates were uniformly low across all models, reflecting the shared use of BVC-based collision avoidance. Importantly, the HP model achieved performance comparable to the HP_{max} configuration, despite using far fewer neurons and markedly lower firing rates, highlighting the efficiency and scalability of the fish-inspired navigation system.

Conclusions

Computational models of spatial navigation have traditionally relied on two major neural components: place cells, which encode location, and grid cells, which provide a metric framework for spatial updating (Dumont and Eliasmith 2020; Komer and Eliasmith 2020). Together, these cell types form the foundation of the mammalian cognitive map (Eichenbaum 2015), often described as an internal GPS that enables efficient navigation and even shortcut planning (Sibeaux et al. 2024). However, recent large-scale electrophysiological studies revealed that the classic place–grid framework does not scale well to complex, naturalistic environments, both spatial patterns and firing properties differ markedly outside of laboratory settings (Eliav et al. 2021; Ginosar et al. 2021, Ginosar et al. 2023).

In teleost fish, which represent the largest vertebrate class, no canonical place or grid cells have been reported. Instead, spatial coding appears to depend primarily on boundary vector cells (BVCs) and hydrostatic-pressure (HP) cues (Cohen et al. 2023; Cohen 2023). To bridge this gap, we developed a neuromorphic spiking neural network (SNN) that emulates the goldfish navigation system, explicitly constrained by electrophysiological data from the telencephalon.

Unlike mammalian models characterized by large neuronal populations and high firing rates, fish possess much smaller populations (on the order of 10^3–10^4 neurons) and significantly lower firing rates (<5 spikes/s; Cohen et al. 2023; Vinepinsky et al. 2020). Accordingly, our model incorporated biologically grounded population sizes, firing rates, and tuning profiles derived from empirical measurements, including BVC, HP, and kinematic neurons (speed, head-direction, velocity).

The virtual environment, a ×32 digital twin of the experimental setup, challenged the simulated fish to locate a food pellet among coral-like obstacles. Performance comparisons among navigation strategies revealed that HP-based navigation yielded consistent and repeatable trajectories (Fig. 3) and significantly outperformed both Null and Azimuth strategies. While HP-guided agents occasionally followed longer routes, their reliability was markedly higher. Crucially, increasing neural population size and firing rate (HP_{max} model) did not improve performance, confirming the efficiency of biologically constrained architectures. The tuned HP model also maintained stable performance across varying task complexities and arena scales (Fig. 3F–I). In natural conditions, fish likely integrate multiple sensory modalities. While HP provides a robust vertical cue, BVC ensembles may contribute to positional inference by encoding relative distances from multiple environmental landmarks, effectively constructing a distributed spatial reference. Future research should explore how combined BVC–HP strategies can support adaptive navigation in dynamic underwater habitats. Our model highlight that compact navigation architectures, such as those observed in fish, can remain both energy-efficient and computationally powerful, offering valuable insight into the evolution of spatial memory and the comparative organization of neural navigation systems across species.

Competing interests

The authors have declared that no competing interests exist.

References

Baxendale, S., and Whitfield, T. T. 2014. Zebrafish inner ear development and function. In Development of Auditory and Vestibular Systems, 63–105. Elsevier.

Bekolay, T.; Bergstra, J.; Hunsberger, E.; DeWolf, T.; Stewart, T. C.; Rasmussen, D.; Choo, X.; Voelker, A. R.; and Eliasmith, C. 2014. Nengo: A Python tool for building large-scale functional brain models. Frontiers in Neuroinformatics 7:48.

Bloch, S.; Hagio, H.; Thomas, M.; Heuzé, A.; Hermel, J.; Lasserre, E.; Colin, I.; Saka, K.; Affaticati, P.; and Jenett, A. 2020. Non-thalamic origin of zebrafish sensory nuclei implies convergent evolution of visual pathways in amniotes and teleosts. Elife 9:e54945.

Broglio, C.; Gómez, A.; Durán, E.; Salas, C.; and Rodríguez, F. 2011. Brain and cognition in teleost fish. In Fish Cognition and Behavior, 325–358. Wiley.

Cohen-Duwek, H., and Ezra Tsur, E. 2021. Biologically plausible spiking neural networks for perceptual filling-in. In Proceedings of the Annual Meeting of the Cognitive Science Society 43(43).

Cohen-Duwek, H.; Slovin, H.; and Ezra Tsur, E. 2022. Computational modeling of color perception with biologically plausible spiking neural networks. PLoS Computational Biology 18(10):e1010648.

Cohen, L.; Vinepinsky, E.; Donchin, O.; and Segev, R. 2023. Boundary vector cells in the goldfish central telencephalon encode spatial information. PLoS Biology 21(4):e3001747.

Conklin, J., and Eliasmith, C. 2005. A controlled attractor network model of path integration in the rat. Journal of Computational Neuroscience 18:183–203.

Davis, V. A.; Holbrook, R. I.; and de Perera, T. B. 2021. Fish can use hydrostatic pressure to determine their absolute depth. Communications Biology 4(1):1–5.

Dumont, N. S.; Orchard, J.; and Eliasmith, C. 2022. A model of path integration that connects neural and symbolic representation. In Proceedings of the Annual Meeting of the Cognitive Science Society 44(44).

Dumont, N., and Eliasmith, C. 2020. Accurate representation for spatial cognition using grid cells. In Proceedings of the Cognitive Science Society.

Ecke, G. A.; Bruijns, S. A.; Hoelscher, J.; Mikulasch, F. A.; Witschel, T.; Arrenberg, A. B.; and Mallot, H. A. 2020. Sparse coding predicts optic flow specificities of zebrafish pretectal neurons. Neural Computing and Applications 32:6745–6754.

Eichenbaum, H. 2015. The hippocampus as a cognitive map... of social space. Neuron 87(1):9–11.

Eliasmith, C., and Anderson, C. H. 2003. Neural Engineering: Computation, Representation, and Dynamics in Neurobiological Systems. MIT Press.

Eliav, T.; Maimon, S. R.; Aljadeff, J.; Tsodyks, M.; Ginosar, G.; Las, L.; and Ulanovsky, N. 2021. Multiscale representation of very large environments in the hippocampus of flying bats. Science 372(6545):eabg4020.

Fernandes, A. M.; Mearns, D. S.; Donovan, J. C.; Larsch, J.; Helmbrecht, T. O.; Kölsch, Y.; Laurell, E.; Kawakami, K.; Dal Maschio, M.; and Baier, H. 2021. Neural circuitry for stimulus selection in the zebrafish visual system. Neuron 109(5):805–822.

Finkelstein, A.; Las, L.; and Ulanovsky, N. 2016. 3-D maps and compasses in the brain. Annual Review of Neuroscience 39:171–196.

Geva-Sagiv, M.; Las, L.; Yovel, Y.; and Ulanovsky, N. 2015. Spatial cognition in bats and rats: From sensory acquisition to multiscale maps and navigation. Nature Reviews Neuroscience 16(2):94–108.

Ginosar, G.; Aljadeff, J.; Burak, Y.; Sompolinsky, H.; Las, L.; and Ulanovsky, N. 2021. Locally ordered representation of 3D space in the entorhinal cortex. Nature 596(7872):404–409.

Ginosar, G.; Aljadeff, J.; Las, L.; Derdikman, D.; and Ulanovsky, N. 2023. Are grid cells used for navigation? On local metrics, subjective spaces, and black holes. Neuron 111(12):1858–1875.

Givon, S.; Altsuler-Nagar, R.; and Segev, R. 2025. The neural substrate of navigation using hydrostatic cues in goldfish. Royal Society Open Science 12(2):241869.

Givon, S.; Pickholtz, R.; Pickholtz, E. Y.; Ben-Shahar, O.; Kiflawi, M.; and Segev, R. 2022. Toward naturalistic neuroscience of navigation: Opportunities in coral reef fish. Frontiers in Neural Circuits 16:895381.

Izhikevich, E. M. 2007. Dynamical Systems in Neuroscience. MIT Press.

Komer, B., and Eliasmith, C. 2020. Efficient navigation using a scalable, biologically inspired spatial representation. In Proceedings of the Cognitive Science Society.

Kubo, F.; Hablitzel, B.; Dal Maschio, M.; Driever, W.; Baier, H.; and Arrenberg, A. B. 2014. Functional architecture of an optic flow-responsive area that drives horizontal eye movements in zebrafish. Neuron 81(6):1344–1359.

McNaughton, B. L.; Battaglia, F. P.; Jensen, O.; Moser, E. I.; and Moser, M.-B. 2006. Path integration and the neural basis of the "cognitive map". Nature Reviews Neuroscience 7(8):663–678.

Moser, E. I.; Kropff, E.; and Moser, M.-B. 2008. Place cells, grid cells, and the brain's spatial representation system. Annual Review of Neuroscience 31:69–89.

Mueller, T. 2012. What is the thalamus in zebrafish? Frontiers in Neuroscience 6:64.

Northcutt, R. G. 2011. Do teleost fishes possess a homolog of mammalian isocortex? Brain, Behavior and Evolution 78(2).

Northmore, D. 2024. Visual shape discrimination in goldfish, modelled with the neural circuitry of optic tectum and torus longitudinalis. Vision Research 217:108374.

O'Keefe, J., and Dostrovsky, J. 1971. The hippocampus as a spatial map: Preliminary evidence from unit activity in the freely-moving rat. Brain Research.

Payne, H. L.; Lynch, G. F.; and Aronov, D. 2021. Neural representations of space in the hippocampus of a food-caching bird. Science 373(6552):343–348.

Pedraja, F.; Hofmann, V.; Lucas, K. M.; Young, C.; Engelmann, J.; and Lewis, J. E. 2018. Motion parallax in electric sensing. Proceedings of the National Academy of Sciences 115(3):573–577.

Reinel, C. P., and Schuster, S. 2018. Rapid depth perception in hunting archerfish II: An analysis of potential cues. Journal of Experimental Biology 221(14):jeb177352.

Ristroph, L.; Liao, J. C.; and Zhang, J. 2015. Lateral line layout correlates with the differential hydrodynamic pressure on swimming fish. Physical Review Letters 114(1):018102.

Rodriguez, F.; Duran, E.; Vargas, J. P.; Torres, B.; and Salas, C. 1994. Performance of goldfish trained in allocentric and egocentric maze procedures suggests the presence of a cognitive mapping system in fishes. Animal Learning and Behavior 22:409–420.

Rodríguez, F.; López, J. C.; Vargas, J. P.; Broglio, C.; Gómez, Y.; and Salas, C. 2002. Spatial memory and hippocampal pallium through vertebrate evolution: Insights from reptiles and teleost fish. Brain Research Bulletin 57(3–4):499–503.

Rosa Salva, O.; Sovrano, V. A.; and Vallortigara, G. 2014. What can fish brains tell us about visual perception? Frontiers in Neural Circuits 8:119.

Rowland, D. C.; Roudi, Y.; Moser, M.-B.; and Moser, E. I. 2016. Ten years of grid cells. Annual Review of Neuroscience 39:19–40.

Schulz-Mirbach, T.; Heß, M.; Metscher, B. D.; and Ladich, F. 2013. A unique swim bladder–inner ear connection in a teleost fish revealed by a combined high-resolution microtomographic and three-dimensional histological study. BMC Biology 11(1):1–13.

Shalumov, A.; Halaly, R.; and Tsur, E. E. 2021. Lidar-driven spiking neural network for collision avoidance in autonomous driving. Bioinspiration and Biomimetics 16(6):066016.

Sibeaux, A.; Newport, C.; Green, J. P.; Karlsson, C.; Engelmann, J.; and Burt de Perera, T. 2024. Taking a shortcut: What mechanisms do fish use? Communications Biology 7(1):578.

Stewart, T.; Choo, X.; and Eliasmith, C. 2010. Symbolic reasoning in spiking neurons: A model of the cortex/basal ganglia/thalamus loop. In Proceedings of the Annual Meeting of the Cognitive Science Society 32(32).

Taylor, G. K.; Holbrook, R. I.; and de Perera, T. B. 2010. Fractional rate of change of swim-bladder volume is reliably related to absolute depth during vertical displacements in teleost fish. Journal of the Royal Society Interface 7(50):1379–1382.

Tsur, E. E. 2021. Neuromorphic Engineering: The Scientist's, Algorithms Designer's and Computer Architect's Perspectives on Brain-Inspired Computing. CRC Press.

Vinepinsky, E.; Cohen, L.; Perchik, S.; Ben-Shahar, O.; Donchin, O.; and Segev, R. 2020. Representation of edges, head direction, and swimming kinematics in the brain of freely navigating fish. Scientific Reports 10(1):1–16.

Wullimann, M. F. 2011. Basal ganglia: Insights into origins from lamprey brains. Current Biology 21(13):R497–R500.

Zhao, D., and Si, B. 2025. Formation of cognitive maps in large-scale environments by sensorimotor integration. Cognitive Neurodynamics 19(1):19.